Universiteit Antwerpen

This item is the archived peer-reviewed author-version of:

Plasma activation of methane for hydrogen production in a N_2 rotating gliding arc warm plasma : a chemical kinetics study

uantwerpen.be

Accepted Manuscript

Plasma activation of methane for hydrogen production in a N_2 rotating gliding arc warm plasma: a chemical kinetics study

Hao Zhang, Weizong Wang, Xiaodong Li, Long Han, Mi Yan, Yingjie Zhong, Xin Tu

Please cite this article as: H. Zhang, W. Wang, X. Li, L. Han, M. Yan, Y. Zhong, X. Tu, Plasma activation of methane for hydrogen production in a N_2 rotating gliding arc warm plasma: a chemical kinetics study, *Chemical Engineering Journal* (2018), doi: https://doi.org/10.1016/j.cej.2018.03.123

Plasma activation of methane for hydrogen production in a N_2 rotating gliding arc warm plasma: a chemical kinetics study

Hao Zhang[a,1,*], Weizong Wang[b,1], Xiaodong Li[a], Long Han[c], Mi Yan[c], Yingjie Zhong[c], Xin Tu[d,*]

[a] *State Key Laboratory of Clean Energy Utilization, Zhejiang University, Hangzhou 310027, China*

[b] *Research group PLASMANT, Department of Chemistry, University of Antwerp, Antwerp 2610, Belgium*

[c] *Institute of Energy and Power Engineering, Zhejiang University of Technology, Hangzhou 310014, China*

[d] *Department of Electrical Engineering and Electronics, University of Liverpool, Liverpool L69 3GJ, UK*

Abstract

In this work, a chemical kinetics study on methane activation for hydrogen production in a warm plasma, i.e., N_2 rotating gliding arc (RGA), was performed for the first time to get new insights into the underlying reaction mechanisms and pathways. A zero-dimensional chemical kinetics model was developed, which showed a good agreement with the experimental results in terms of the conversion of CH_4 and product selectivities, allowing us to get a better understanding of the relative significance of various important species and their related reactions to the formation and loss of CH_4, H_2, and C_2H_2 etc. An overall reaction scheme was obtained to provide a realistic picture of the plasma chemistry. The results reveal that the electrons and excited nitrogen species (mainly $N_2(A)$) play a dominant role in the initial dissociation of CH_4. However, the H atom induced reaction $CH_4 + H \rightarrow CH_3 + H_2$, which has an enhanced reaction rate due to the high gas temperature (over 1200 K), is the major contributor to both the conversion of CH_4 and H_2 production, with its relative contributions of >90% and >85%, respectively, when only considering the forward reactions. The coexistence and interaction of thermochemical and plasma chemical processes in the rotating gliding arc warm plasma significantly enhance the process performance. The formation of C_2 hydrocarbons follows a nearly one-way path of $C_2H_6 \rightarrow C_2H_4 \rightarrow C_2H_2$, explaining why the selectivities of C_2 products decreased in the order of $C_2H_2 > C_2H_4 > C_2H_6$.

---

[1] The two authors contributed equally to this work.

* Corresponding Authors:

E-mails: zhanghao900320@gmail.com (H. Zhang), xin.tu@liverpool.ac.uk (X. Tu)

1. Introduction

The increasing pressure of diminishing fossil fuel reserves coupled with the issue of global warming, has motivated the development of affordable energy carriers that are renewable and environment-friendly. Hydrogen is one of the most promising alternative energy sources that may play a key role in various specialized areas such as fuel cells, combustion engines, and gas turbines [1-5]. Currently the catalytic methane steam reforming process is the most well-developed technique for hydrogen production [6]. However, the relatively low specific productivity, large equipment size, and high temperature requirement (600-1000 K), as well as the rapid deactivation of catalysts in the reforming process, still limit its industrial applications, particularly in small-scale distributed and mobile systems where rapid ignition/response is essential [7-9].

In this respect, plasma technology, and more specifically atmospheric pressure non-thermal plasma, is gaining increasing attention for hydrogen production from methane activation [4, 7, 10-13]. Non-thermal plasma offers numerous highly reactive species (e.g., energetic electrons, radicals, and excited species) that are responsible for the initiation and propagation of chemical reactions whereby expensive and impurity vulnerable catalyst can be eliminated, while maintaining a limited energy cost due to the relatively low gas temperature and good chemical selectivity [14-18]. High reaction rate, fast attainment of steady state, and high specific productivity ensure rapid start-up and shutdown of the plasma process, providing flexible integration into small-scale hydrogen production systems [15, 19-21]. In addition, these merits allow non-thermal plasma systems to utilize electricity from intermittent renewable sources, e.g., solar and wind, offering a solution to the imbalance between energy production and consumption by renewable sources [22]. Various atmospheric pressure non-thermal plasmas have been investigated for methane conversion, such as dielectric barrier discharge (DBD) [19, 23], corona discharge [24], and glow discharge [25], however, the relatively low energy density in these plasmas makes it difficult to achieve a high conversion at higher feed flow rates [10].

Warm plasma, a transitional discharge that exhibits a relatively higher gas temperature (e.g., 1000-4000 K) and a higher power (e.g., 30-500W), such as gliding arc discharge, spark discharge, and microwave discharge that are generated with the stabilization by power or current constraints, show significantly higher energy efficiency for various fuel reforming processes in comparison to other non-thermal plasmas, especially at high feed flow rates. As proposed by Gangoli, Gutsol, and Fridman et al., transitional warm plasma systems are probably optimal for large-scale fuel reforming

2

[26-28]. In our previous study [29], a novel rotating gliding arc (RGA) warm plasma was developed for hydrogen production from methane activation in N_2, exhibiting significant advantages in terms of CH_4 conversion (maximum, 91.8%), hydrogen selectivity (maximum, 80.7%), and hydrogen energy yield (maximum, 22.6 g/kWh) with a feed flow rate of several orders of magnitude higher than that of typical non-thermal plasmas (e.g., DBD).

However, most of the current research in this field is based on experiments and assumptions without an in-depth understanding of the ongoing plasma chemical reactions [26, 27, 30-32]. The underlying mechanisms of this energy-efficient process in warm plasmas are still far from understood, which is severely limiting the scale-up and application of this promising technology. To the best of our knowledge, no chemical modeling investigation on fuel reforming processes in warm plasmas has been reported.

In this work the methane activation reaction in the N_2 RGA warm plasma was selected for chemical kinetics study, in order to provide new insights into the underlying mechanisms of fuel reforming processes in warm plasmas. A zero-dimensional (0-D) chemical kinetics model was developed to describe the plasma chemistry. The calculated CH_4 conversion and product selectivities at various CH_4/N_2 molar ratios were compared with the experimental results for the validation of the model. It is worth mentioning that a more extensive experimental study is beyond the scope of our current work and the reader can refer to our previous publication [29] for details. Based on this model, the plasma chemistry of various species was elucidated with main attention devoted to the conversion of CH_4 and production of two major products, H_2 and C_2H_2. The relative contributions of competing formation and loss paths for these species were investigated as a function of CH_4/N_2 molar ratio. To provide a realistic picture of the plasma chemistry, the overall reaction mechanisms of the plasma process were schematically illustrated.

2. Description of the model

2.1 Chemical kinetics model

The procedure for the 0-D chemical kinetics modeling is schematically shown in Fig. 1. Both electron-impact reactions and heavy particle (i.e., atoms, molecules, radicals, ions, and excited species) reactions that are considered to be competing in the plasma chemistry were included in the model. It was calculated by means of an Boltzmann solver, i.e. BOLSIG+ [33], based on the collision cross sections (σ) as well as the reduced electric field and gas temperature, which were obtained

experimentally by means of oscilloscope and optical emission spectroscopy (OES), respectively (as reported in our previous study [29]). Note that the reduced electric field was obtained from the average value of the voltage. The gas temperatures of plasma under the studied conditions are given in Table 1. The Arrhenius rate coefficient of heavy particle reactions depends on gas temperature, and the parameters were adopted from literature and NIST Chemical Kinetics Database (see the Supplementary Material) [34].

Table 1 The gas temperatures of plasma at different CH_4/N_2 molar ratios

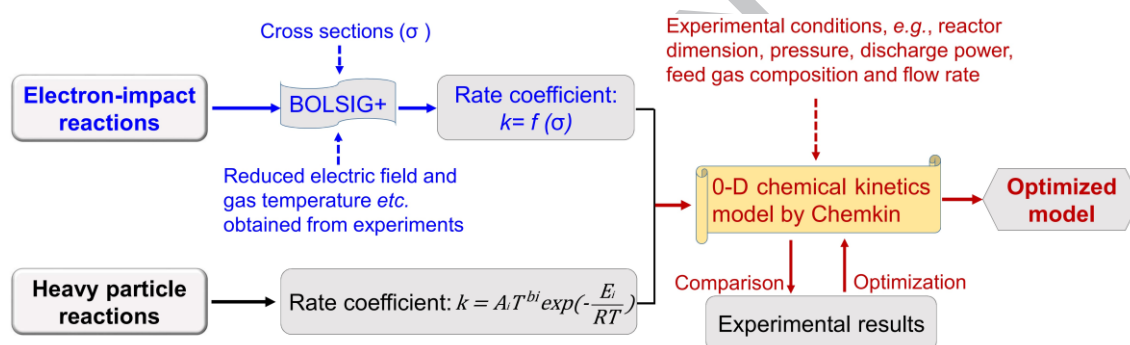| CH_4/N_2 molar ratio	0.05	0.10	0.20	0.04	0.60	0.80	1.00	1.20
Gas temperature (K)	1528	1359	1328	1298	1256	1230	1206	1200

Fig. 1 Procedure for the chemical kinetics modeling

By providing a set of gas reactions and the experimental conditions (e.g., reactor dimension, pressure, discharge power, feed gas composition and flow rate), the model was then implemented in the Plasma PSR (perfectly stirred reactor) module of Chemkin software [35], which is a well-developed and commonly used proprietary software tool for basic kinetics simulations. After a comparison of the simulations with the experimental results, an optimization of the model was conducted using a better choice of the cross section or rate coefficient obtained from different literature sources. Known from the high-speed frames of the discharge, the plasma was around 10 mm in thickness, yielding a reactor volume of around 3.6 ml. The discharge power input was obtained based on the electrical parameters measured by oscilloscope. Under the studied conditions, the discharge power is in the range of 315 - 397 W and the corresponding specific energy input (ratio of discharge power to feed flow rate) is 3.15 - 3.97 kJ/l. All plasma properties and species densities were assumed to be uniform throughout the entire reactor volume and the plasma process was determined primarily

by chemical kinetics rather than by species transport in the reactor. The 0-D model described herein focused mainly on the details of the plasma physics and plasma chemistry but neglected the sophisticated dimensional effects and surface kinetics in plasma.

A total of 32 species have been included in this model, as shown in Table 2. These species react with each other through 120 electron-impact reactions and 166 heavy particle reactions. Note that excited species (e.g., $N_2(B^3\Pi_g)$ and $N_2(C^3\Pi_u)$, see Table S1) are only included in the model to describe the energy loss processes, and thus not treated as separate species here. Additionally, we have omitted ions such as CH_2^+ and C^+ from the model and the reactions which result in the formation of these ions have also not been taken into account in the particle balance equations. However, these reactions have been included in the cross-section database in order to calculate the electron energy distribution function (EEDF) correctly. Similar method has been used in the literature [36]. The full list of all the reactions can be found in the Supplementary Material (Table S1 and S2). A more detailed description of the 0-D model is available in the literature [37, 38] and in the Supplementary Material.

Table 2 Overview of the species included in the model

Molecules	Radicals	Excited species	Charged species
CH_4, C_2H_6, C_2H_4, C_2H_2, C_3H_4, C_3H_6, C_3H_8	CH_3, CH_2, CH, C_2H_5, C_2H_3, C_2H, C_2, C, C_3H_7, C_3H_5, C_3H_2		e
H_2	H		
N_2	N	$N_2(A^3\Sigma_u^+)$, $N_2(a'^1\Sigma_u^-)$ $N(^4S)$, $N(^2D)$	
HCN	CN		
NH_3	NH, NH_2		

The average electron density was assumed to be constant in the simulation of each case and the similar method has been used by Kozák et al. in the modeling of CO_2 conversion by a microwave discharge system [36]. Previous studies [39, 40] showed that a RGA plasma has an electron density of $10^{12} \sim 10^{14}$ cm^{-3}, and our previous experimental study [29] gives an electron density of around 10^{13} cm^{-3}. Therefore, we assumed the average electron density is 10^{13} cm^{-3} at a CH_4/N_2 molar ratio of 1.0

in the model. The used values of electron density for other CH_4/N_2 molar ratios were slightly adjusted based on the calculation of Snoeckx et al. [41].

2.2 Electron-impact reactions

Electron-impact reactions are considered as the initial step of plasma chemistry, contributing to both the direct decomposition of methane, and production of various chemically reactive excited species (e.g., $N_2(A)$, $N(^4S)$), which play a significant role in the propagation of plasma chemical reactions. The presence of a variety of collision processes and numerous species in the plasma chemical process remains a significant challenge for modeling. It is difficult to include all the collisions in the model, and a simplification by considerably reducing the negligible reactions is necessary. In this model, the dominant electron-impact reactions such as momentum transfer, electronic excitation, vibrational excitation, rotational excitation, dissociation, and ionization processes of the main species, i.e., N_2, CH_4, H_2, C_2H_6, C_2H_5, C_2H_4, C_2H_3, C_2H_2, C_2H, CH_3, CH_2, and CH were taken into account. According to previous study [37], the electron attachment processes for the production of negative ions were neglected. Table S1 lists the electron-impact reactions included in the model with the sources of the cross sections.

2.3 Heavy particle reactions

The existing atoms, molecules, radicals, ions, and excited species can react with each other, contributing significantly to the generation of products (e.g., H_2, C_2H_2, and C_2H_4). According to the experimental results and previous studies, 31 types of heavy particle species including excited nitrogen species, H_2, H, C_mH_n ($1 \leq m \leq 3$, $0 \leq n \leq 2m+2$), and neutral nitrogen species were taken into account in this model, yielding 166 heavy particle reactions. The rate coefficients together with the corresponding references are also listed in the Supplementary Material (see Table S2). Considering the limited number density of ions occurring in the discharge plasma due to the relatively low electron energy in the RGA plasma (a mean electron temperature of around 1 eV), the ion involved heavy particle reactions were not included in the simulation, which is in consistent with other works [38, 42, 43]. In addition, the three-body collisions are considered to be negligible and were not taken into account [10, 38, 44]. Different types of heavy particle reactions are introduced in detail as follow.

Excited nitrogen species

In plasma bulk, the electron-impact reactions of background gas N_2 can produce a variety of excited nitrogen species, such as N_2 ($C^3\Pi_u$) ($N_2(C)$), N_2 ($B^3\Pi_g$) ($N_2(B)$), N_2 ($A^3\Sigma_u^+$) ($N_2(A)$), N_2 ($a'^1\Sigma_u^-$) ($N_2(a')$), N_2^+ ($B^2\Sigma_u^+$) ($N_2^+(B)$), $N(^4S)$, $N(^2D)$, and $N(^2P)$ etc. [41, 42, 45-50]. A reasonable elimination of reactions that are of little importance is normally required based on the density and lifetime of the excited species, as well as the rate coefficients of the related reactions.

Our previous study [29] showed that, the spectrum of the N_2 RGA was dominated by the radiative species such as $N_2(C)$, $N_2(B)$, and $N_2^+(B)$. Nevertheless, the radiative lifetimes of these species are very short in atmospheric pressure plasmas [50, 51], thus significantly limiting their contribution to the chemical reactivity of the N_2 plasma. Therefore, these species were not considered in this model, which is commonly seen in other modeling studies of CH_4/N_2 plasmas [41, 46, 50]. The metastable $N_2(A)$ is produced from the electron-impact excitation of N_2 and also radiatively from $N_2(B)$. The threshold energy of $N_2(A)$ at zero vibrational level ($v = 0$) is 6.17 eV [41], which is sufficient to break CH_4 bond (the dissociation energy of C-H is 4.5 eV). In addition, the radiative lifetime of $N_2(A)$ is up to around 2s [52]. Therefore, $N_2(A)$ is probably of great importance for the methane decomposition process. In an experimental study by Golde et al. [53], the formation of H_2 was clearly observed in consequence of the collisions of CH_4 with $N_2(A)$ ($v = 0-6$).

The metastable $N_2(a')$, which has a high energy level of 8.52 eV, together with a relatively long lifetime of 13-500 μs, is also considered as an important intermediate species. In a microwave discharge used for methane decomposition in N_2 by Pintassilgo et al. [45], the $N_2(a')$ induced reaction $CH_4 + N_2(a') \rightarrow N_2 + C + H_2 + H_2$ (R130 in Table S2) exhibited a small contribution to methane conversion at a pressure of 2670 Pa. Snoeckx et al. performed a modeling study on a DBD based methane conversion into H_2 in N_2, showing that with increasing N_2 concentration to 30%, $N_2(a')$ played an increasing role in the production of H_2 via reaction R130 [41].

In addition, the metastable excited $N(^4S)$ and $N(^2D)$ atoms in the plasma present a relatively high rate coefficient for the reactions with CH_4, CH_3 etc. [41, 45-47, 50, 54, 55], and thus cannot be ignored as well. The excited $N(^2P)$ atom was proven to be substantially less reactive with methane than $N(^2D)$ (around 60 times less) [49], and was consequently not considered in the simulation.

Based on the above analysis, the excited $N_2(A)$ and $N_2(a')$ molecules, together with the excited atoms $N(^4S)$ and $N(^2D)$ were included in the model. Note that the $N_2(A)$ in Table S2 represents the

$N_2(A)$ species with vibrational levels of $v = 0$-9.

H_2, H, and C_mH_n $(1 \leq m \leq 3, 0 \leq n \leq 2m+2)$

A significant number of reactions among H_2, H, and hydrocarbons or radicals including CH_4, CH_3, CH_2, CH, C_2H_6, C_2H_5, C_2H_4, C_2H_3, C_2H_2, C_2H, C_2, C, C_3H_8, C_3H_7, C_3H_6, C_3H_5, C_3H_4 and C_3H_2 were taken into account in the model. The C_4 or higher hydrocarbons involved reactions were assumed to be negligible, considering their low yields. As known from our previous OES study [29], the RGA CH_4/N_2 warm plasma exhibits a gas temperature of over 1200 K, which is higher than the thermal decomposition temperature of CH_4 molecules (around 930 K). Consequently, the thermal decomposition reactions, which were normally ignored in typical non-thermal systems [41, 47, 48, 50], were considered in the warm plasma chemistry.

Neutral nitrogen species

Our previous results showed that CN and HCN were experimentally detected as an important intermediate and gas product, respectively [29]. In addition, trace NH_3 was also found in other experimental work [41]. Therefore, the neutral nitrogen-containing species N, CN, HCN, NH, NH_2, and NH_3 have also been included in the model.
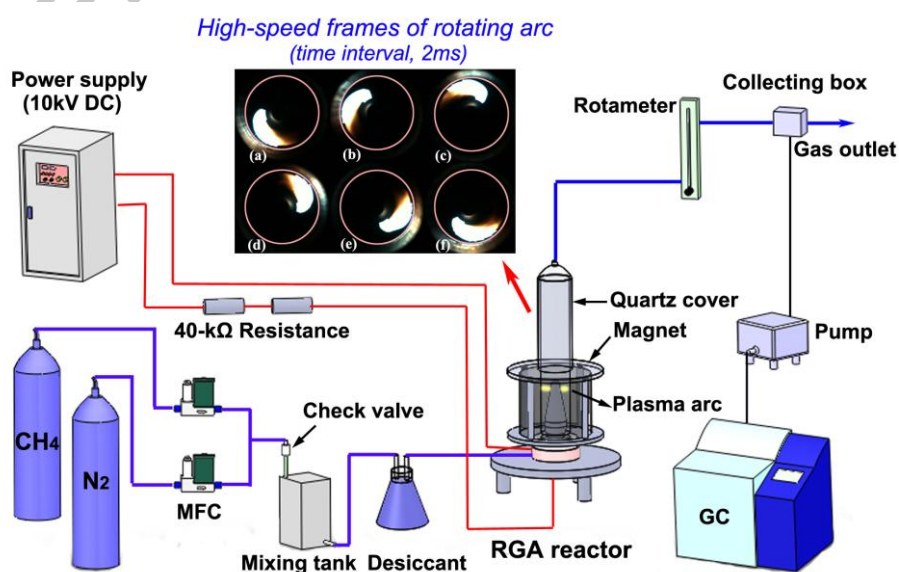
3. Experimental section

Fig. 2 Schematic diagram of the experimental setup

The experiments were carried out at atmospheric pressure using a homemade RGA reactor [29], as shown in Fig. 2. The reactor consisted of a con-shaped inner electrode and a circular outer electrode, both of which were made of stainless steel. The inner electrode was connected to a high-voltage source (positive bias) while the outer electrode was grounded, providing a narrowest discharge gap of 2 mm for the initial ignition of the arc. The reactor was powered by a customized 10 kV DC power supply and a 40-kΩ resistance was connected in series in the circuit to limit and stabilize the current. A magnet was placed outside of the ground electrode, generating an upward magnetic field inside the reactor for the stabilization and acceleration of the arc. Three tangential inlets were designed at the bottom of the reactor for the injection of reactants (CH_4/N_2), ensuring the formation of a swirling flow inside the reactor. The arc was initiated at the narrowest gap, then moved upward and finally rotated rapidly around the inner electrode as a result of the combined effect of Lorentz force and swirling flow, thus generating a stable plasma volume for chemical reactions. Each experiment was repeated three times with similar results and the averaged values are given.

The gaseous products were analyzed using a gas chromatography (GC, Fuli Analytical Instrument GC9790A) equipped with a thermal conductivity detector (TCD) for the detection of H_2 and N_2, as well as a flame ionization detector (FID) for the measurement of hydrocarbons. A 5A molecular sieve packed column (2 m $\times$ 3 mm, helium carrier gas) was used for the TCD detector, while a GDX-104 packed column (2 m $\times$ 3 mm, helium carrier gas) was chosen for the FID detector. The column temperature was set at 300 K for the gas analysis. The GC was calibrated for a wide range of concentrations for each gaseous component using reference gas mixtures (Shanghai Weichuang Standard Gas Analytical Technology Co., Ltd.) and other calibrated gas mixtures. The CH_4 conversion and product selectivity (H_2 and C_mH_n) are defined as follows:

$$CH_4 \text{ conversion } (\%) = \frac{\text{mol of } CH_4 \text{ converted}}{\text{mol of } CH_4 \text{ introduced}} \times 100\% \tag{1}$$

$$H_2 \text{ selectivity } (\%) = \frac{(\text{mol of } H_2 \text{ produced}) \times 2}{(\text{mol of } CH_4 \text{ converted}) \times 4} \times 100\% \tag{2}$$

$$C_mH_n \text{ selectivity } (\%) = \frac{(\text{mol of } C_mH_n \text{ produced}) \times m}{\text{mol of } CH_4 \text{ converted}} \times 100\% \tag{3}$$

A set of experimental results [29] at an applied voltage of 10 kV, a flow rate of 6 l/min, and an

external resistance of 40 kΩ were selected to be compared with our calculated results by the plasma kinetics model.

4. Results and Discussion

4.1 Validation of the model

A comparison of the simulated and experimental CH_4 conversion is plotted as a function of CH_4/N_2 molar ratio in Fig. 3, showing a good agreement with a relative error below 10.1%. The agreement between the simulation and experimental results is reached in a more extensive range of operating parameters (for example at different gas flow rates, see Fig. S1 in the Supplementary Material). For the sake of clarity, in the following section, we only presented the results at various CH_4/N_2 molar ratios to provide a realistic picture of the plasma chemistry.
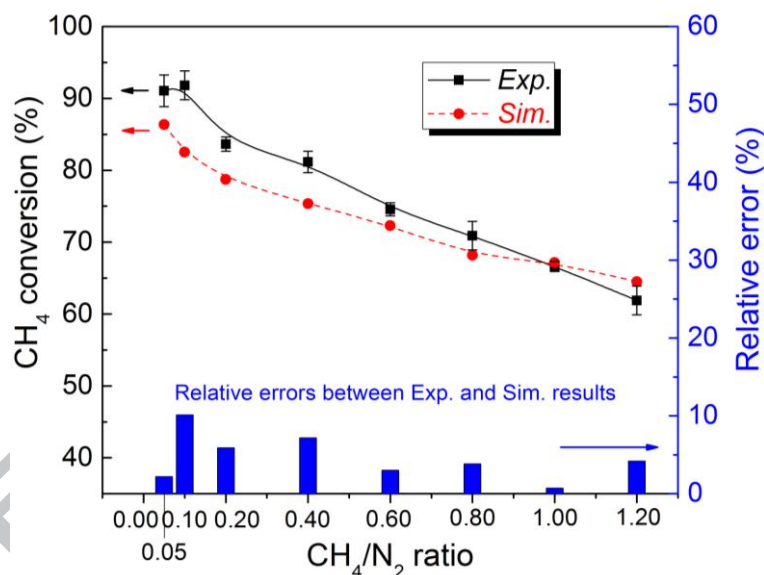

Fig. 3 Simulated and experimental CH_4 conversion, together with the corresponding relative error as a function of CH_4/N_2 molar ratio

Further validation of the model is performed through a comparison between the simulated and experimental selectivity of gas products, as shown in Fig. 4. In addition, typical measured and calculated outlet gas compositions are listed in Table 3. All the simulated results show a fairly good agreement with the experimental ones. H_2 is the main gas product with a concentration of around one order of magnitude higher than that of C_2H_2. The predicted concentration of C_2H_6 was 0.01-0.02%, whereas no C_2H_6 was detected in the experiment, which could be due to the high detection limit of the GC. Similar trends of H_2, C_2H_2, and C_2H_6 selectivity between the simulated and experimental

data upon increasing the CH_4/N_2 molar ratio can be seen in Fig. 4, except for the C_2H_2 selectivity in the region of $CH_4/N_2 = 0.05$-0.20.
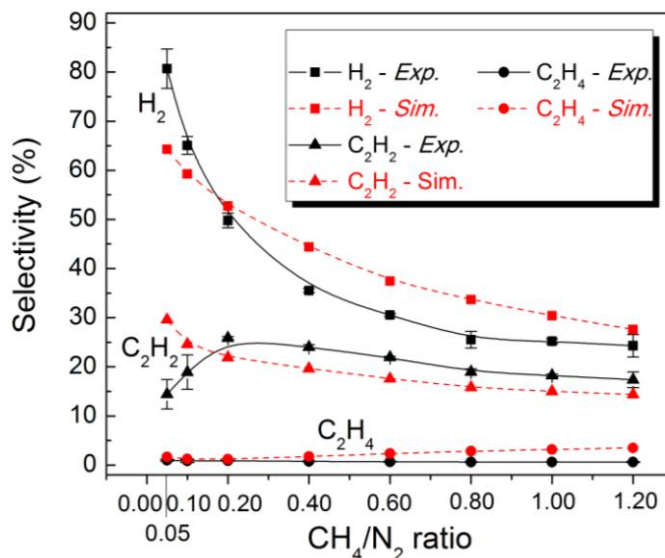

Fig. 4 Simulated and experimental selectivity of gas products as a function of CH_4/N_2 molar ratio

Table 3 Comparison of simulated and experimental outlet gas compositions under typical conditions

Component	$CH_4/N_2 = 0.20$		$CH_4/N_2 = 0.40$	
	Exp. (vol. %)	Sim. (vol. %)	Exp. (vol. %)	Sim. (vol. %)
CH_4	2.73	3.48	5.38	6.36
N_2	75.48	77.87	69.75	64.39
H_2	13.89	13.99	16.48	21.92
C_2H_2	1.80	1.33	2.78	1.91
C_2H_4	0.06	0.07	0.09	0.17
C_2H_6	0.00	0.01	0.00	0.02

The discrepancy between the modeling and experimental results could be attributed to the following effects. Firstly, carbon formation in the methane conversion was assumed to be in the gas phase to simplify the 0-D model. However, carbon deposition was observed on the walls of the RGA reactor, thus carbon balance was not 100%. Secondly, some of the available reaction rate coefficients included in this model are prone to some deviations. Furthermore, an uncertainty exists in the experiment resulted from the complexity of plasma chemical process, as stated by some authors [56].

Overall, the calculated and experimental results are in rather good agreement, certainly in view of the complexity of the plasma chemistry, indicating that the model can provide a more or less realistic picture of the plasma chemistry, and therefore can be used to elucidate the underlying reaction mechanisms and pathways in the plasma activation of methane.

4.2 Conversion of CH_4

Fig. 5 shows the dominant reactions with a relative contribution of higher than 0.1% together with the reaction rates for the conversion and formation of CH_4 ($CH_4/N_2 = 0.10$). Furthermore, the relative contributions of the key pathways with a relative contribution of higher than 1% are plotted in Fig. 6 as a function of CH_4/N_2 molar ratio. Clearly, the H atom induced reaction R166 is the dominant reaction for the overall conversion of CH_4 with a relative contribution of over 90% under all of the tested conditions. Interestingly, the importance of reaction R166 in the conversion of CH_4 was also reported by Legrand et al. using a microwave N_2 plasma [57].

$$CH_4 + H \rightarrow CH_3 + H_2 \hspace{4cm} R166$$

The reaction of C_2H_3 with CH_4 (R164) is also responsible for the conversion of CH_4 to some extent (2.4-4.8%).

$$CH_4 + C_2H_3 \rightarrow C_2H_4 + CH_3 \hspace{4cm} R164$$
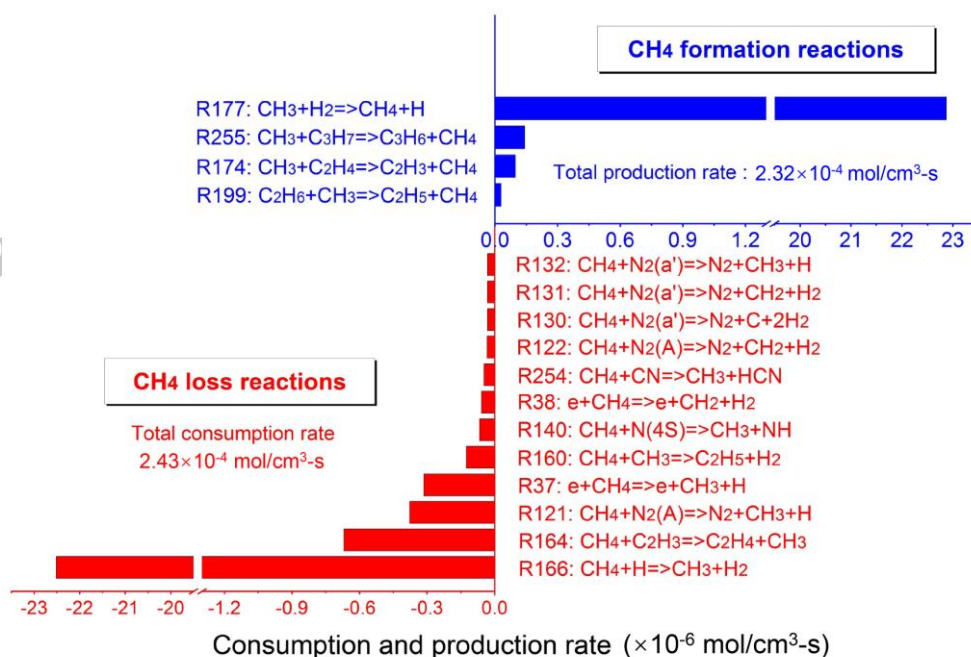

Fig. 5 Dominant reaction pathways and corresponding reaction rates for the formation and loss of CH_4 ($CH_4/N_2 = 0.10$) (For the figures hereinafter, the formation and loss reaction rates of

12

corresponding species are positive and negative, respectively; the reaction numbers are taken from Tables S1 and S2.)
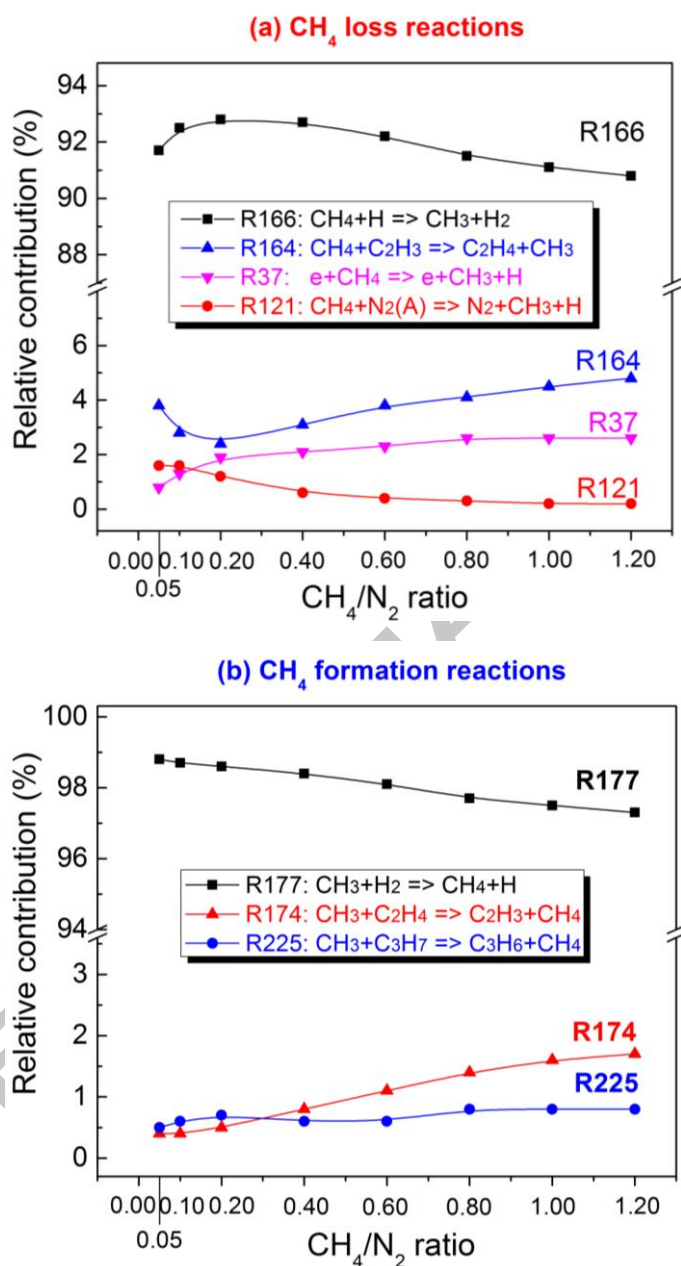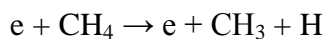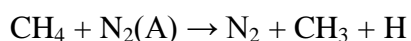

Fig. 6 Relative contributions of the most important paths for the loss (a) and formation (b) of CH_4 as a function of CH_4/N_2 molar ratio.

The highly energetic electrons and metastable $N_2(A)$ play predominant roles in the initial dissociation of CH_4 via the electron impact reaction R37 and $N_2(A)$ induced reaction R121, respectively.

$$e + CH_4 \rightarrow e + CH_3 + H \hspace{4cm} R37$$

13

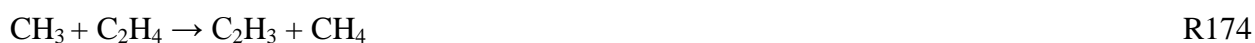$$CH_4 + N_2(A) \rightarrow N_2 + CH_3 + H \qquad\qquad\qquad R121$$

The relative contribution of the above two pathways to the overall CH_4 conversion is 0.8-2.6% and 1.6-0.2%, respectively. At a CH_4/N_2 molar ratio below 0.10, $N_2(A)$ is more important for the initial dissociation of CH_4. However, with the increase of CH_4/N_2 molar ratio, the role of $N_2(A)$ in the dissociation of CH_4 declines in contrast to that of electron due to the drop in $N_2(A)$ density and increase in electron density [41]. In the experiment [29], we found that decreasing N_2 concentration (and $N_2(A)$) reduced the conversion of CH_4. The following combined effects are associated with these phenomena: (a) the decreasing electron density with increasing N_2 content (also see [41]) lowers the contribution of the electron impact reactions to both the CH_4 loss and H_2 production (R37); and (b) with the increase of N_2 content, the role of N_2 metastable states becomes more important and Penning dissociation reactions with CH_4 become important for CH_4 loss and H_2 formation (R121). Note that the combined effects may enhance the net loss reaction rate of CH_4 with increasing CH_4/N_2 molar ratio (as seen from Fig. 7). However, a decreased CH_4 conversion can still be obtained because the increasing feed CH_4 amount cannot be compensated by the increasing loss reaction rate. Similar results were also reported in methane conversion using a N_2 DBD plasma [41].

Note that $N_2(A)$ has been widely reported as a key specie in the processing of hydrocarbons in nitrogen plasmas. Legrand et al. [49] reported that $N_2(A)$ was more important for the dissociation of methane in comparison to electrons and excited N atoms in a N_2 microwave plasma. Pintassilgo et al. [45, 46] found that in the post-discharge of a microwave N_2 plasma, the decomposition of CH_4 was primarily attributed to the reaction with $N_2(A)$ to produce CH_3 and CH_2 (CH_4 concentration <1%). Aerts et al. developed a kinetics model to understand the reaction mechanisms in the destruction of C_2H_4 in a N_2 DBD plasma [58]. They found that $N_2(A)$ made a significant contribution (31%) to the direct destruction of C_2H_4 with a concentration of 100 ppm at a specific energy density of 600 mJ/cm^3.

As shown in Fig. 6(b), CH_4 can be formed through the reactions of CH_3 radicals with H_2 (R177), C_2H_4 (R174), and C_3H_7 (R225) with R177 being the dominant pathway having a relative contribution of up to 97.3-98.8%.

$$CH_3 + C_2H_4 \rightarrow C_2H_3 + CH_4 \qquad\qquad\qquad R174$$

$$CH_3 + H_2 \rightarrow CH_4 + H \qquad\qquad\qquad R177$$

$$CH_3 + C_3H_7 \rightarrow C_3H_6 + CH_4 \qquad\qquad\qquad R225$$
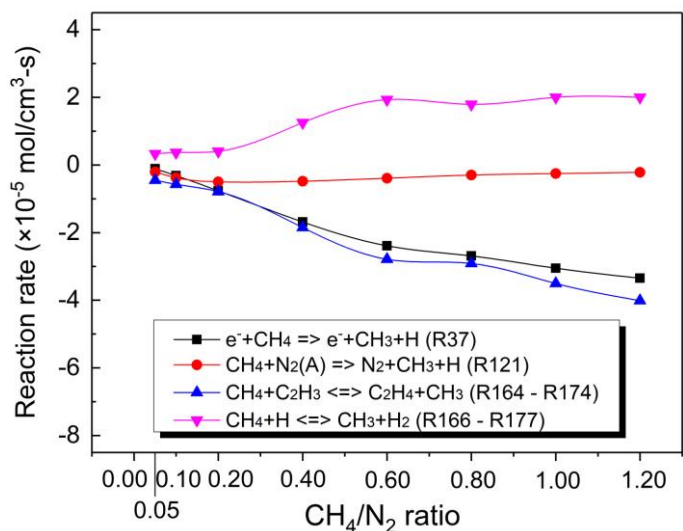
14

Fig. 7 Net reactions rates of various CH_4 conversion processes as a function of CH_4/N_2 molar ratio.

Although the collision between CH_4 and H (R166) is the dominant reaction for CH_4 conversion (Fig. 6(a)), it is worth noting that the reaction R166 (and its reverse reaction) has an overall negative net contribution to the conversion of CH_4 (Fig. 7) if considering its reverse reaction R177 that has a much higher reaction rate. This finding indicates that there is more CH_4 formed from CH_3 than vice versa. In contrast, the rate of reaction R164 is much higher than that of its reverse reaction R174, and thus, reaction R164 has a largest net contribution to the conversion of CH_4 under the tested conditions in this work, as clearly indicated in Fig. 7.

4.3 Production of H_2

Fig. 8 shows the important formation and loss reactions of H_2 (relative contribution >0.1%) at a CH_4/N_2 molar ratio of 0.10. The relative contributions of the key reaction pathways (relative contribution >1%) are plotted in Fig. 9. Clearly, R166 is also the dominant reaction for the formation of H_2 with a relative contribution of over 85.9%. Interestingly, Indarto et al. reported similar findings in the decomposition of methane using a traditional gliding arc reactor [44]. Moreover, the H atom induced reactions with C_2H_4, C_3H_8, and C_2H_6 etc. can also contribute to the formation of H_2 via the following reactions, of which reaction R212 shows a relatively high contribution of 3.4-5.7%.
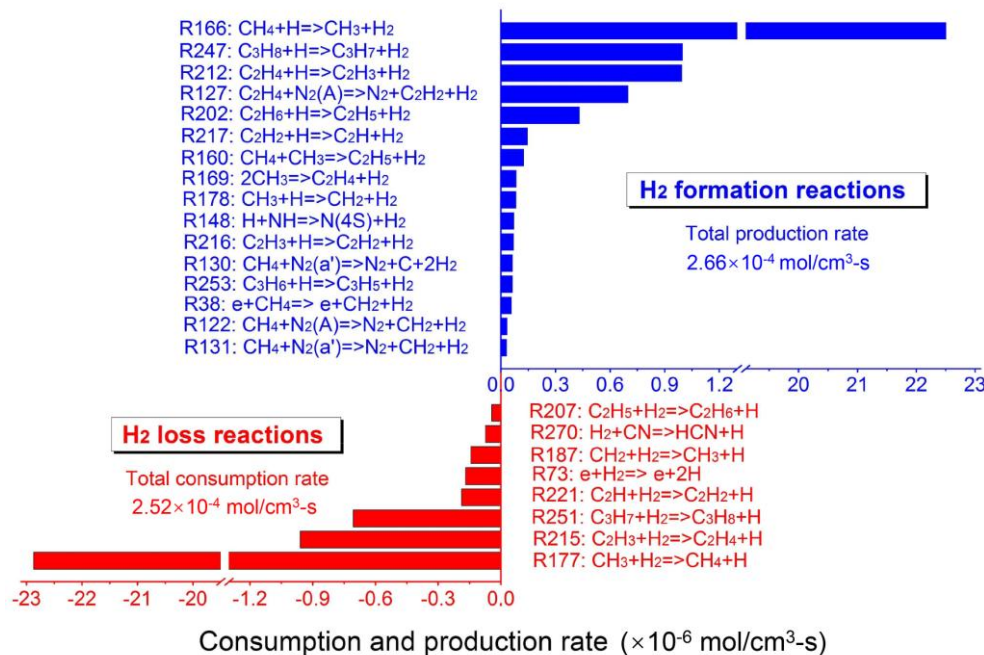
$$C_2H_6 + H \rightarrow C_2H_5 + H_2 \qquad\qquad\qquad\qquad R202$$

$$C_2H_4 + H \rightarrow C_2H_3 + H_2 \qquad\qquad\qquad\qquad R212$$

$$C_3H_8 + H \rightarrow C_3H_7 + H_2 \qquad\qquad\qquad\qquad R247$$

15

Fig. 8 Dominant pathways and corresponding reaction rates for the formation and loss of H_2 (CH_4/N_2 = 0.10)

However, it is worth mentioning that the reaction R166 (and its reverse reaction) has an overall negative net contribution to the formation of H_2 as a result of a larger reaction rate of its reverse reaction R177 (see Fig. 10). In contrast, the dominant net contributions to the formation of H_2 come from the collisions of C_2H_4, C_3H_8, and C_2H_6 species with H atoms when the CH_4/N_2 molar ratio is higher than 0.40.
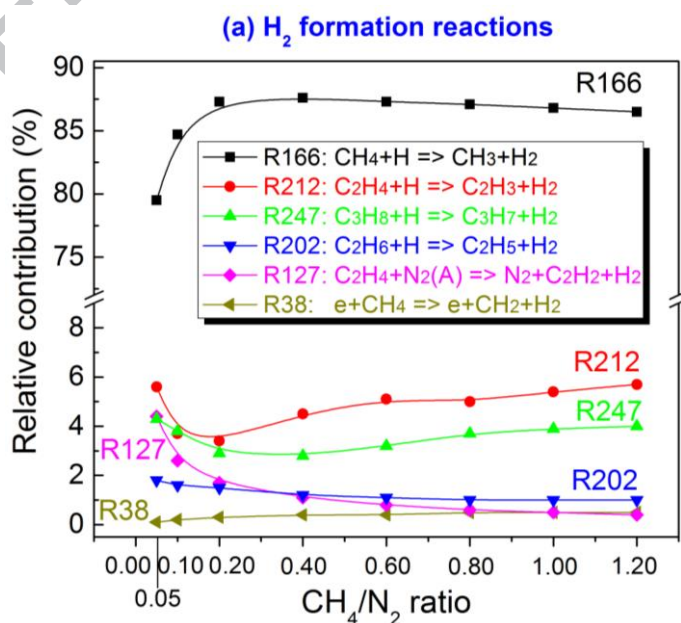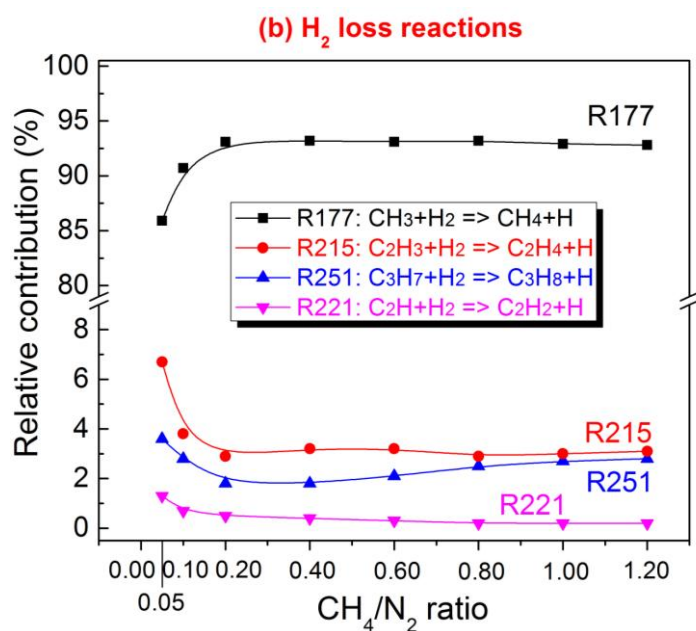
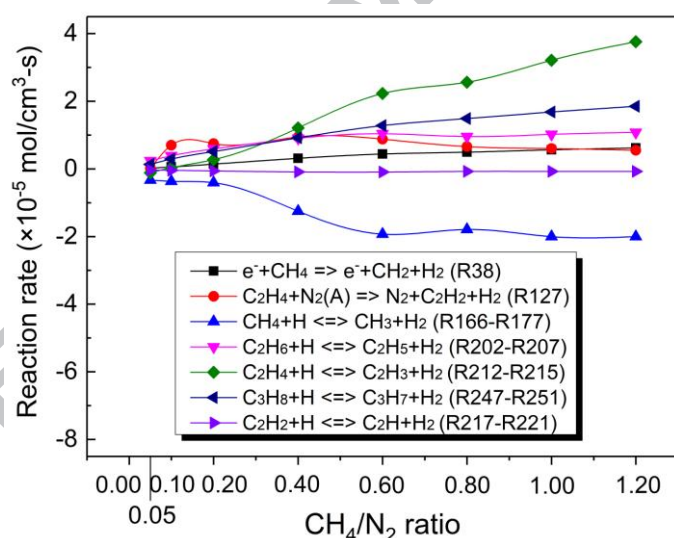**Fig. 9** Relative contributions of the most important paths for the formation (a) and loss (b) of H_2 as a function of CH_4/N_2 molar ratio

Fig. 10 Net reactions rates of various H_2 production processes as a function of CH_4/N_2 molar ratio.

Moreover, the dissociation of CH_4 and C_2H_4 stimulated by electrons and N_2 (A), respectively, has a minor contribution to the production of H_2 via reactions R38 and R127 (0.1-0.5% and 0.4-4.4%, respectively) as indicated in Fig. 9(a) if only the forward reaction rates are included. Increasing CH_4/N_2 molar ratio reduced the contribution of R127 but increased that of R38 for H_2 production. When the reverse reaction rates are included, our calculations clearly indicate that the collision of C_2H_4 upon N_2 (A) is the most important net process for H_2 formation when the CH_4/N_2 molar ratio is

17

lower than 0.20 (see Fig. 10).

$$e + CH_4 \rightarrow e + CH_2 + H_2 \qquad\qquad R38$$

$$C_2H_4 + N_2(A) \rightarrow N_2 + C_2H_2 + H_2 \qquad\qquad R127$$

In this study, if only the forward reactions are included, the role of H atom is of primary importance both for the overall conversion of CH_4 and for the production of H_2 due to the reaction R166: $CH_4 + H \rightarrow CH_3 + H_2$. When the reverse reactions are taken into account, the net contributions of the reactions involving neutral species collisions to the overall conversion of CH_4 and production of H_2 are still more important than that of the electrons and excited nitrogen species. Although the electrons and excited nitrogen species (mainly $N_2(A)$) are dominant for the initial dissociation of CH_4, their contributions to the overall CH_4 conversion and H_2 production are fairly low. Whereas, Snoeckx et al. [41] reported that in a DBD plasma, the $N_2(A)$ involved reaction R121: $CH_4 + N_2(A) \rightarrow N_2 + CH_3 + H$ was the most important pathway for the overall CH_4 conversion with a relative contribution of up to 25-45% and the electron-impact reaction R37: $e + CH_4 \rightarrow e + CH_3 + H$ also provided a significant contribution of 5-25% for CH_4 dissociation. For the production of H_2 in their study, the $N_2(a')$ involved CH_4 dissociation reaction R130: $CH_4 + N_2(a') \rightarrow N_2 + C + H_2 + H_2$ was shown to be the most important with a relative contribution of 40-65%. Yang et al. [37] performed a modeling study for the decomposition of pure CH_4 in a DBD plasma, and results showed that the electron-impact CH_4 dissociation R37: $e + CH_4 \rightarrow e + CH_3 + H$ was the primary pathway for the overall CH_4 conversion.

It is clear that the electron and excited nitrogen species (e.g., $N_2(A)$ and $N_2(a')$) generated by DBD plasmas play a more important role in the dissociation of CH_4 compared to the RGA warm plasma. This is logical, because the RGA plasma has a mean electron energy of around 1 eV, which is significantly lower than that reported in DBD plasmas (2-3 eV) [41], limiting both electron-impact dissociation of CH_4 and electron-impact excitation of nitrogen molecules. More importantly, the DBD plasma had a relatively low gas temperature and, for example, the rate coefficient of reaction R166: $CH_4 + H \rightarrow CH_3 + H_2$ was set as a constant of $k = 8.43 \times 10^{-19}$ $cm^3 \cdot s^{-1}$ at 300K in their model, resulting in a limited reaction rate of reaction R166. Whereas, in our model, the rate coefficient of R166 was 6.62×10^{-21} $T^{3.2}$ exp (-36.6/RT) (R = 8.314 $\times 10^{-3}$ kJ mol^{-1} K^{-1}) which is

temperature-dependent. Due to the high gas temperature of the RGA plasma (over 1200 K), reaction R166 has a considerably high reaction rate, and thus plays a dominant role in the dissociation of CH_4 in the RGA plasma. It is also interesting to note that, the experimentally obtained CH_4 conversion in the RGA plasma (maximum, 91.8%) is remarkably higher than that in the DBD plasma (maximum, $\approx 12.0\%$) [41] whilst maintaining a total flow rate of one order of magnitude higher.

The comparison of experimental and calculated results between the RGA warm plasma and other non-thermal plasmas enables us to make a plausible conclusion that an efficient conversion of methane in plasma is difficult to be achieved solely by electrons and/or excited species induced methane dissociation. A relatively high gas temperature makes a significant contribution to achieving a desired methane conversion due to the enhanced rate coefficients of reactions driven by heavy particles as a result of thermal effect. This is potentially why warm plasma, a transitional discharge that exhibits a relatively higher gas temperature (e.g., 1000-4000K), such as RGA, microwave discharge, and spark that are generated with the stabilization by power or current constraints, show significantly higher energy efficiency for fuel reforming processes in comparison to traditional non-thermal plasmas such as DBD [20, 21, 27, 30-32, 59, 60]. For instance, in a heat-insulated gliding arc warm plasma used for oxidative pyrolysis reforming of methanol, an energy cost of 1-2 orders of magnitude lower than that of typical non-thermal plasmas (e.g., corona) can be achieved with a considerably high energy efficiency of 74% [31].

Warm plasmas typically operate at significantly higher power (e.g., 30-500W) and higher gas temperature (e.g., 1000-4000K) in comparison to other non-thermal plasmas, while maintaining better chemical selectivity and lower energy consumption than that of thermal plasmas [26, 29, 61]. The above results show that the coexistence and interaction of thermochemical and plasma chemical processes in the warm plasma significantly enhance the process performance [60].

4.4 Production of C_2H_2

Figs. 11 and 12 show the competing formation and loss reactions (relative contribution >0.1%) of another main product C_2H_2 ($CH_4/N_2 = 0.10$), as well as the relative contributions of the predominant reactions (relative contribution >1%) as a function of CH_4/N_2 molar ratio. The production of C_2H_2 is mainly attributed to the following pathways, of which the $N_2(A)$ induced dissociation of C_2H_4 (reaction R127) is dominant.

$$C_2H_4 + N_2(A) \rightarrow N_2 + C_2H_2 + H_2 \qquad\qquad R127$$

$C_2H_5 + C_2H_3 \rightarrow C_2H_6 + C_2H_2$ R204

$C_2H_3 + H \rightarrow C_2H_2 + H_2$ R216

$C_2H + H_2 \rightarrow C_2H_2 + H$ R221
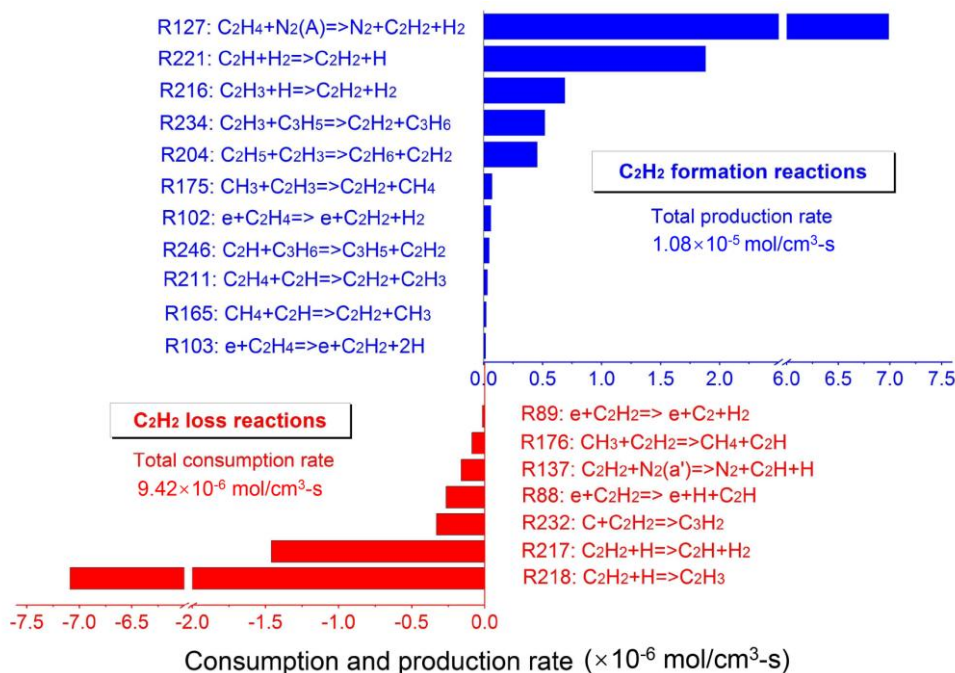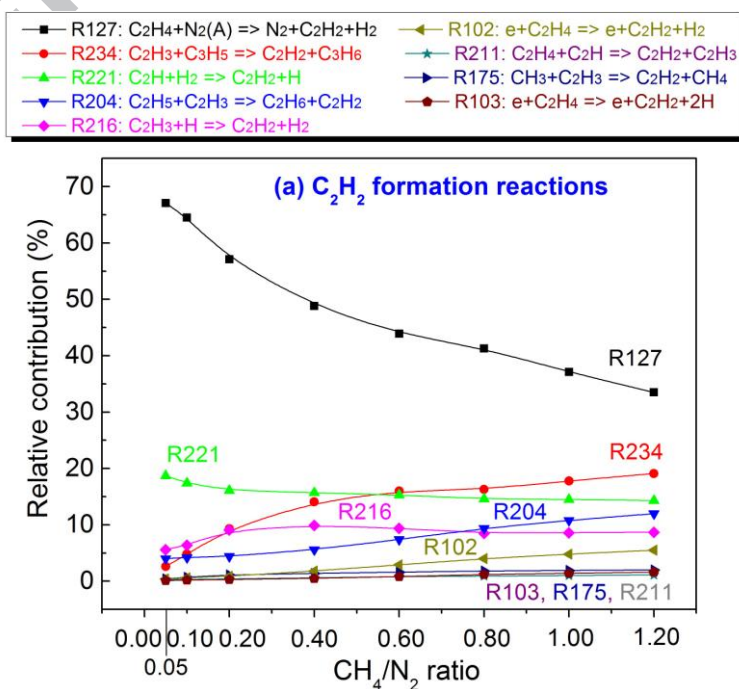
$C_2H_3 + C_3H_5 \rightarrow C_2H_2 + C_3H_6$ R234

Fig. 11 Dominant pathways and corresponding reaction rates for the formation and loss of C_2H_2 ($CH_4/N_2 = 0.10$)
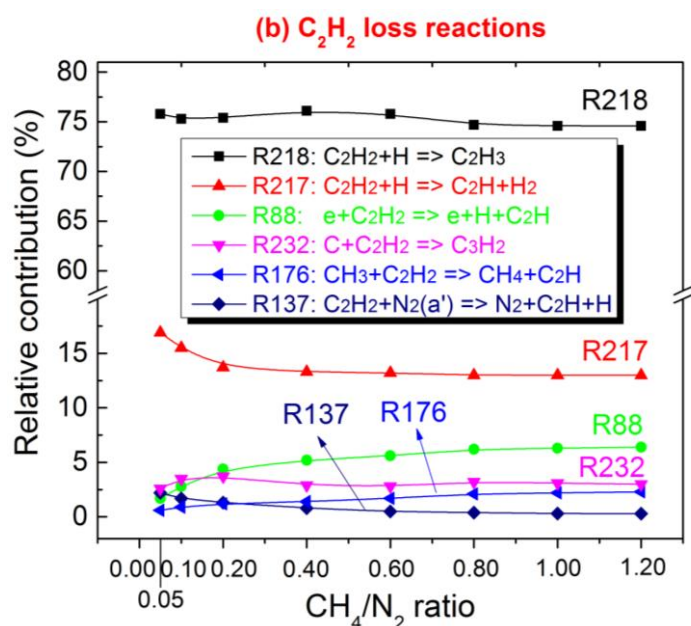
Fig. 12 Relative contributions of the most important paths for the formation (a) and loss (b) of C_2H_2 as a function of CH_4/N_2 molar ratio

Increasing CH_4/N_2 molar ratio from 0.05 to 1.2 leads to a continuous drop of the relative contribution of reaction R127 from 67.1% to 33.5%, as shown in Fig. 12(a). The electron-impact dissociation of C_2H_4 (R102: $e + C_2H_4 \rightarrow C_2H_2 + H_2$) also made a minor contribution to the formation of C_2H_2 (0.4% to 5.5%).

The loss of C_2H_2 was principally driven by hydrogenation reaction (R218), with a relative contribution of 74.6-76.1%.

$$C_2H_2 + H \rightarrow C_2H_3 \hspace{4cm} \text{R218}$$

4.5 Overall reaction mechanisms

The detailed formation and loss reaction mechanisms of trace products, such as C_2H_4, C_2H_6, and HCN, are not presented in this paper. To gain better insights into the underlying reaction mechanisms in this reforming process, an overall reaction scheme of the plasma chemistry is schematically depicted in Fig. 13.

The starting step of the plasma chemistry is from the electron-impact reactions of CH_4 and N_2, resulting in the initial dissociation of CH_4 and the production of excited nitrogen species, such as $N_2(A)$, $N_2(a')$, and $N(^4S)$ (especially $N_2(A)$), which will subsequently contribute to the dissociation of CH_4. The heavy particle reactions of CH_4 with H atoms that have significantly high reaction rates

21

due to the high gas temperature in the RGA plasma, can contribute significantly to the efficient conversion of CH_4, if only the forward reactions are included.
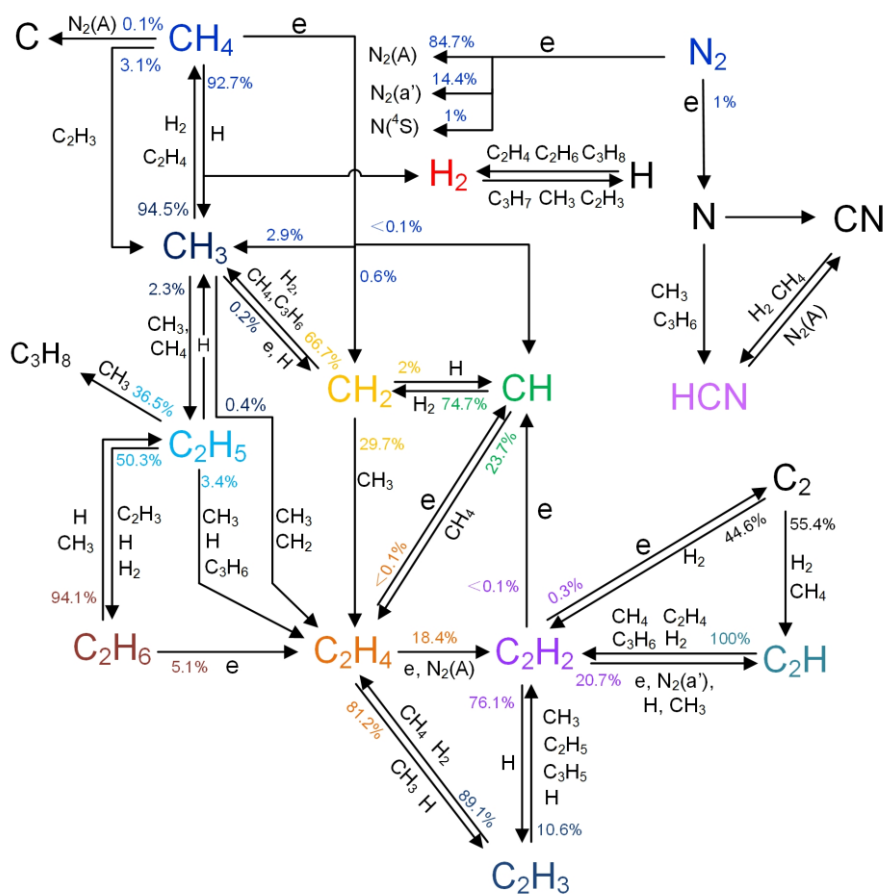

Fig. 13 Reaction scheme to illustrate the dominant pathways of the plasma chemistry in RGA plasma assisted CH_4 decomposition process in N_2. The percentages on the arrowed lines represent the relative contributions of different paths for the depletion of corresponding species at $CH_4/N_2 = 0.40$.
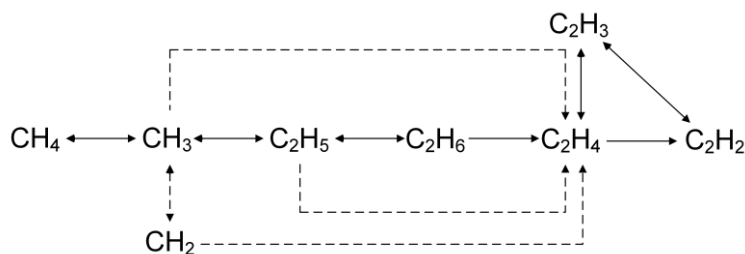

Fig. 14 Dominant reaction paths for the formation of C_2 hydrocarbons. The dashed lines represents the paths with minor contributions.

A mechanism schematic focusing on the reaction paths of C_2 hydrocarbons is presented in Fig. 14. As shown in Figs. 13 and 14, CH_3 radicals produced from CH_4 conversion play a predominant role in

the subsequent formation of C_2H_2, C_2H_4, and C_2H_6 etc. Fig. 14 indicates that the formation of C_2 hydrocarbons follows a nearly one-way path of $C_2H_6 \rightarrow C_2H_4 \rightarrow C_2H_2$ with negligible backward reactions. This is why the selectivity of C_2 hydrocarbons in the experiment decreased in the following order: $C_2H_2 > C_2H_4 > C_2H_6$. Similar formation paths of C_2 hydrocarbons have been reported in the decomposition of pure CH_4 using DBD plasmas [62, 63].

The electron-impact dissociation of N_2 produces N atoms which contributed to the formation of major N-containing product HCN.

5. Conclusions

In this study, a zero-dimensional chemical kinetic model was developed to obtain a better insight into the underlying mechanisms of methane activation for hydrogen production in a N_2 rotating gliding arc (RGA) warm plasma. Both competing electron-impact and heavy particle (i.e., atoms, molecules, radicals, ions, and excited species) reactions were considered in the model and a reasonable agreement between the calculated and experimental CH_4 conversion and product selectivities was achieved. The relative contributions of various important species and their related reactions for the conversion of CH_4 and production of main products H_2 and C_2H_2 were investigated as a function of CH_4/N_2 ratio.

Results revealed that, although the electrons and metastable $N_2(A)$ were the dominant species in the initial dissociation of CH_4, their contributions to the overall CH_4 conversion were minor, which were only 0.8-2.6% and 1.6-0.2%, respectively. Increasing CH_4/N_2 ratio resulted in an increase in the role of electron but a drop in that of $N_2(A)$ for CH_4 conversion.

The H atom involved reaction $CH_4 + H \rightarrow CH_3 + H_2$, which had a significantly high reaction rate due to the high gas temperature of the RGA warm plasma (over 1200 K), played a dominant role for both the conversion of CH_4 and the production of H_2 with relative contributions of >90% and >85%, respectively. However, it is worth mentioning this reaction has an overall negative net contribution to the CH_4 conversion, if its reverse reaction with much higher reaction rate is considered. In contrast, the collision of CH_4 upon C_2H_3 has a dominant net contribution to the overall CH_4 conversion if both the forward and reverse reaction rates are taken into account. Additionally, the collisions of C_2H_4, C_3H_8, and C_2H_6 species with H atoms lead to a largest net contribution to H_2 production when the CH_4/N_2 ratio is higher than 0.40, and the collision of C_2H_4 upon excited $N_2(A)$ gives the dominant

23

contribution to H_2 production when the CH_4/N_2 ratio is lower than 0.20. Warm plasmas are probably optimal for large-scale fuel reforming in consequence of the coexistence and interaction of thermochemical and plasma chemical processes, which allows for a high efficiency of the process even at higher flow rate.

Another main product C_2H_2 was formed primarily from C_2H_4 via the $N_2(A)$ involved reaction $C_2H_4 + N_2(A) \rightarrow N_2 + C_2H_2 + H_2$. The overall reaction mechanisms indicated that the formation of C_2 hydrocarbons followed a nearly one-way path of $C_2H_6 \rightarrow C_2H_4 \rightarrow C_2H_2$, explaining why the experimentally obtained selectivities of C_2 hydrocarbons decreased in the following order: $C_2H_2 > C_2H_4 > C_2H_6$.

Acknowledgements

References

[1] J. Yeston, Sourcing hydrogen directly from wax. Science 354 (2016) 594-595.

[2] C.M. Du, J.M. Mo, H.X. Li, Renewable hydrogen production by alcohols reforming using plasma and plasma-catalytic technologies: challenges and opportunities. Chem. Rev. 115 (2014) 1503-1542.

[3] K.C. Kwon, S. Choi, K. Hong, C.W. Moon, Y.S. Shim, D.H. Kim, T. Kim, W. Sohn, J.M. Jeon, C.H. Lee, K.T. Nam, S. Han, S.Y. Kim, H.W. Jang, Wafer-scale transferable molybdenum disulfide thin-film catalysts for photoelectrochemical hydrogen production. Energ. Environ. Sci. 9 (2016) 2240-2248.

[4] O. Khalifeh, H. Taghvaei, A. Mosallanejad, M.R. Rahimpour, A. Shariati, Extra pure hydrogen production through methane decomposition using nanosecond pulsed plasma and Pt–Re catalyst. Chem. Eng. J. 294 (2016) 132-145.

[5] P. Nikolaidis, A. Poullikkas, A comparative overview of hydrogen production processes. Renew. Sust. Energ. Rev. 67 (2017) 597-611.

[6] D. Jantke, L. Pardatscher, M. Drees, M. Cokoja, W.A. Herrmann, F.E. Kühn, Hydrogen production and storage on a formic acid/bicarbonate platform using water-soluble N-Heterocyclic carbene complexes of late transition metals. ChemSusChem 9 (2016) 2849-2854.

[7] H.L. Chen, H.M. Lee, S.H. Chen, Y. Chao, M.B. Chang, Review of plasma catalysis on hydrocarbon reforming for hydrogen production—interaction, integration, and prospects. Appl. Catal. B-Environ. 85 (2008) 1-9.

[8] C.H. Tsai, K.T. Chen, Production of hydrogen and nano carbon powders from direct plasmalysis of methane. Int. J. Hydrogen Energ. 34 (2009) 833-838.

[9] B. Wang, B. Sun, X. Zhu, Z. Yan, Y. Liu, H. Liu, Q. Liu, Hydrogen production from alcohol solution by microwave discharge in liquid. Int. J. Hydrogen Energ. 41 (2016) 7280-7291.

[10] M. Garduño, M. Pacheco, J. Pacheco, R. Valdivia, A. Santana, B. Lefort, N. Estrada, C. Riverarodríguez,

24

Hydrogen production from methane conversion in a gliding arc. J. Renew. Sustain. Ener. 4 (2012) 1.

[11] O. Khalifeh, A. Mosallanejad, H. Taghvaei, M.R. Rahimpour, A. Shariati, Decomposition of methane to hydrogen using nanosecond pulsed plasma reactor with different active volumes, voltages and frequencies. Appl. Energ. 169 (2016) 585-596.

[12] M. Shirazi, E.C. Neyts, A. Bogaerts, DFT study of Ni-catalyzed plasma dry reforming of methane. Appl. Catal. B-Environ. 205 (2017) 605-614.

[13] W.C. Chung, M.B. Chang, Simultaneous generation of syngas and multiwalled carbon nanotube via CH_4/CO_2 reforming with spark discharge. ACS Sustain. Chem. Eng. 5 (2017) 206-212.

[14] W.Z. Wang, B.S. Patil, S. Heijkers, V. Hessel, A. Bogaerts, Nitrogen fixation by gliding arc plasma: better insight by chemical kinetics modelling. ChemSusChem 10 (2017) 2145-2157.

[15] B. Ogungbesan, R. Kumar, L. Su, M. Sassi, Experimental validation of local thermal equilibrium in a MW plasma torch for hydrogen production. Int. J. Hydrogen Energ. 38 (2013) 15210-15218.

[16] W.Z. Wang, D.H. Mei, X. Tu, A. Bogaerts, Gliding arc plasma for CO_2 conversion: better insights by a combined experimental and modelling approach. Chem. Eng. J. 330 (2017) 11-25.

[17] L. Wang, Y.H. Yi, C.F. Wu, H.C. Guo, X. Tu, One-step reforming of CO_2 and CH_4 into High-value liquid chemicals and fuels at room temperature by plasma-driven catalysis. Angew. Chem. Int. Edit. 56 (2017) 13679-13683.

[18] S.Y. Liu, D.H. Mei, Z. Shen, X. Tu, Nonoxidative conversion of methane in a dielectric barrier discharge reactor: Prediction of reaction performance based on neural network model. J. Phys. Chem. C. 118 (2014) 10686-10693.

[19] X. Tu, J.C. Whitehead, Plasma dry reforming of methane in an atmospheric pressure AC gliding arc discharge: co-generation of syngas and carbon nanomaterials. Int. J. Hydrogen Energ. 39 (2014) 9658-9669.

[20] H. Zhang, X.D. Li, F.S. Zhu, K.F. Cen, C.M. Du, X. Tu, Plasma assisted dry reforming of methanol for clean syngas production and high-efficiency CO_2 conversion, Chem. Eng. J. 310 (2017) 114-119.

[21] H. Zhang, X.D. Li, F.S. Zhu, Z. Bo, K.F. Cen, X. Tu, Non-oxidative decomposition of methanol into hydrogen in a rotating gliding arc plasma reactor. Int. J. Hydrogen Energ. 40 (2015) 15901-15912.

[22] R. Snoeckx, A. Ozkan, F. Reniers, A. Bogaerts, The quest for value-added products from carbon dioxide and water in a dielectric barrier discharge: A chemical kinetics study. ChemSusChem 10 (2016) 409-424.

[23] X. Zheng, S. Tan, L. Dong, S. Li, H. Chen, Silica-coated $LaNiO_3$ nanoparticles for non-thermal plasma assisted dry reforming of methane: Experimental and kinetic studies. Chem. Eng. J. 265 (2015) 147-156.

[24] F. Ravari, S.M. Fazeli, H.R. Bozorgzadeh, J. Sadeghzadeh Ahari, Kinetic model study of dry reforming of methane using cold plasma. Phys. Chem. Res. 5 (2017) 395-408.

[25] D. Li, X. Li, M. Bai, X. Tao, S. Shang, X. Dai, Y. Yin, CO_2 reforming of CH_4 by atmospheric pressure glow discharge plasma: a high conversion ability. Int. J. of Hydrogen Energ. 34 (2009) 308-313.

[26] S.P. Gangoli, Experimental and modeling study of warm plasmas and their applications. Ph.D. Dissertation, Drexel University, Philadelphia, 2007.

[27] A. Gutsol, A. Rabinovich, A. Fridman, Combustion-assisted plasma in fuel conversion. J. Phys. D Appl. Phys. 44 (2011) 274001.

[28] A. Gutsol, Warm discharges for fuel conversion. In Handbook of combustion; Lackner, M., Winter F., Agarwal A. K., Eds.; Wiley-VCH: Weinheim, Germany, 2010.

[29] H. Zhang, C.M. Du, A.J. Wu, Z. Bo, J.H. Yan, X.D. Li, Rotating gliding arc assisted methane decomposition in nitrogen for hydrogen production. Int. J. Hydrogen Energ. 39 (2014) 12620-12635.

[30] J. Pacheco, G. Soria, M. Pacheco, R. Valdivia, F. Ramos, H. Frías, M. Durán, M. Hidalgo, Greenhouse gas treatment and H_2 production, by warm plasma reforming. Int. J. Hydrogen Energ. 40 (2015) 17165-17171.

[31] H.Y. Lian, X.S. Li, J.L. Liu, X. Zhu, A.M. Zhu, Oxidative pyrolysis reforming of methanol in warm plasma for an on-board hydrogen production, Int. J. Hydrogen Energ. 42 (2017) 13617-13624..

[32] K. Li, J.L. Liu, X.S. Li, X. Zhu, A.M. Zhu, Warm plasma catalytic reforming of biogas in a heat-insulated reactor: Dramatic energy efficiency and catalyst auto-reduction, Chem. Eng. J. 288 (2016) 671-679.

[33] G. Hagelaar, L. Pitchford, Solving the Boltzmann equation to obtain electron transport coefficients and rate coefficients for fluid models. Plasma Sources Sci. Technol. 14 (2005) 722.

[34] NIST Chemical Kinetics Database, http://kinetics.nist.gov/kinetics/index.jsp.

[35] Chemkin-Pro, Reaction Design, San Diego, 2009.

[36] T. Kozák, A. Bogaerts, Evaluation of the energy efficiency of CO_2 conversion in microwave discharges using a reaction kinetics model, Plasma Sources Sci. Technol. 24 (2014) 015024.

[37] Y. Yang, Direct non-oxidative methane conversion by non-thermal plasma: modeling study. Plasma Chem. Plasma P. 23 (2003) 327-346.

[38] H. Zheng, Q. Liu, Kinetic study of nonequilibrium plasma-assisted methane steam reforming, Math. Probl. Eng. 2014 (2014) 938618.

[39] A. Fridman, A. Gutsol, S. Gangoli, Y. Ju, T. Ombrello, Characteristics of gliding arc and its application in combustion enhancement, J Propul. Power 24 (2008) 1216-1228.

[40] S.P. Gangoli, A.F. Gutsol, A.A. Fridman, A non-equilibrium plasma source: magnetically stabilized gliding arc discharge: II. Electrical characterization, Plasma Sources Sci. Technol. 19 (2010) 065004.

[41] R. Snoeckx, M. Setareh, R. Aerts, P. Simon, A. Maghari, A. Bogaerts, Influence of N_2 concentration in a CH_4/N_2 dielectric barrier discharge used for CH_4 conversion into H_2, Int. J. Hydrogen Energ. 38 (2013) 16098-16120.

[42] J. Legrand, A. Diamy, R. Hrach, V. Hrachova, Kinetics of reactions in $CH_4\backslash N_2$ afterglow plasma: a simplified model. Vacuum 50 (1998) 491-495.

[43] K. Hiraoka, K. Aoyama, K. Morise, A study of reaction mechanisms of methane in a radio-frequency glow discharge plasma using radical and ion scavengers. Can. J. Chem. 63 (1985) 2899-2905.

[44] A. Indarto, J.W. Choi, H. Lee, H.K. Song, Kinetic modeling of plasma methane conversion using gliding arc. J. Nat. Gas Chem. 14 (2005) 13-21.

[45] C. Pintassilgo, C. Jaoul, J. Loureiro, T. Belmonte, T. Czerwiec, Kinetic modelling of a N_2 flowing microwave discharge with CH_4 addition in the post-discharge for nitrocarburizing treatments. J. Phys. D Appl. Phys. 40 (2007) 3620.

[46] C. Pintassilgo, J. Loureiro, Kinetic study of a N_2–CH_4 afterglow plasma for production of N-containing hydrocarbon species of Titan's atmosphere. Adv. Space. Res. 46 (2010) 657-671.

[47] C. Pintassilgo, J. Loureiro, G. Cernogora, M. Touzeau, Methane decomposition and active nitrogen in a N_2-CH_4 glow discharge at low pressures. Plasma Sources Sci. Technol. 8 (1999) 463.

[48] J.C. Legrand, A.M. Diamy, R. Hrach, V. Hrachova, Methane conversion in the flowing afterglow of a dinitrogen microwave plasma: initiation of the reaction. Contrib. Plasma Phys. 37 (1997) 521-537.

[49] J.-C. Legrand, A.M. Diamy, R. Hrach, V. Hrachová, Kinetics of reactions in CH_4/N_2 afterglow plasma. Vaccum 48 (1997) 671-675.

[50] A. Oumghar, J. Legrand, A. Diamy, N. Turillon, R. Ben-Aim, A kinetic study of methane conversion by a dinitrogen microwave plasma. Plasma Chem. Plasma P. 14 (1994) 229-249.

[51] A.M. Harling, J.C. Whitehead, K. Zhang, NOx formation in the plasma treatment of halomethanes. J. Phys. Chem. A 109 (2005) 11255-11260.

[52] M.F. Golde, Reactions of $N_2(A^3\Sigma_u^+)$. Int. J. Chem. Kinet. 20 (2004) 75-92.

[53] M. Golde, G. Ho, W. TAO, J. Thomas, Collisional deactivation of $N_2(A^3\Sigma_u^+, v=0-6)$ by CH_4, CF_4, H_2, H_2O, CF_3Cl, and CF_2HCl. J. Phys. Chem. 93 (1989) 1112-1118.

[54] C. Pintassilgo, J. Loureiro, Production of hydrocarbons and nitriles using a N_2–CH_4 afterglow plasma for simulation of Titan's atmosphere. Planet. Space Sci. 57 (2009) 1621-1630.

[55] K.J. Pringle, J.C. Whitehead, J.J. Wilman, J. Wu, The chemistry of methane remediation by a non-thermal

atmospheric pressure plasma. Plasma Chem. Plasma P. 24 (2004) 421-434.

[56] R. Snoeckx, S. Heijkers, K. Van Wesenbeeck, S. Lenaerts, A. Bogaerts, CO_2 conversion in a dielectric barrier discharge plasma: N_2 in the mix as a helping hand or problematic impurity?. Energ. Environ. Sci. 9 (2016) 999-1011.

[57] J.C. Legrand, A.M. Diamy, R. Hrach, V. Hrachová, Mechanisms of methane decomposition in nitrogen afterglow plasma. Vacuum 52 (1999) 27-32.

[58] R. Aerts, X. Tu, C. De Bie, J.C. Whitehead, A. Bogaerts, An investigation into the dominant reactions for ethylene destruction in non- thermal atmospheric plasmas. Plasma Prcess. Polym. 9 (2012) 994-1000.

[59] H. Zhang, F.S. Zhu, X.D. Li, K.F. Cen, C.M. Du, X. Tu, Enhanced hydrogen production by methanol decomposition using a novel rotating gliding arc discharge plasma. RSC Adv. 6 (2016) 12770-12781.

[60] D.H. Lee, K.T. Kim, Y.-H. Song, W.S. Kang, S. Jo, Mapping plasma chemistry in hydrocarbon fuel processing processes. Plasma Chem. Plasma P. 33 (2013) 249-269.

[61] H. Zhang, F.S. Zhu, X.D. Li, K.F. Cen, C.M. Du, X. Tu, Rotating gliding arc assisted water splitting in atmospheric nitrogen. Plasma Chem. Plasma P. 36 (2016) 813-834.

[62] S.S. Kim, H. Lee, J.W. Choi, B.K. Na, H.K. Song, Kinetics of the methane decomposition in a dielectric-barrier discharge. J. Ind. Eng. Chem. 9 (2003) 787-791.

[63] A. Indarto, N. Coowanitwong, J.W. Choi, H. Lee, H.K. Song, Kinetic modeling of plasma methane conversion in a dielectric barrier discharge. Fuel Process. Technol. 89 (2008) 214-219

Highlights

- Modeling study on methane activation in warm plasma is conducted for the first time

- Electrons and $N_2(A)$ are the dominant species in the initial dissociation of CH_4.

- H atoms play the dominant role for the conversion of CH_4 and the production of H_2.

- Thermochemistry and plasma chemistry coexist in warm plasma.

- The C_2 hydrocarbons form following a nearly one-way path of $C_2H_6 \rightarrow C_2H_4 \rightarrow C_2H_2$.